P3A.3

Variable pulse repetition frequency for the GPM dual-frequency radar

Satoru Kobayashi and Toshio Iguchi

Communications Research Laboratory

1 Introduction

In space missions, the delay of a receiving signal to a transmission signal generally spans a few thousands microseconds due to long range observation. An efficient sampling can be achieved by transmitting pulses successively, as schematically shown in Fig. 1. For the later consideration, a catching integer n is to be introduced. In Fig. 1, the catching integer n is set at 11, for which a pulse transmitted on time 0 is received between the 10th and 11th pulse transmissions, and a pulse on time 1 is received between the 11th and 12th pulses, and so forth. In the GPM as well as the TRMM, the range varies from one swing angle to another, accompanied with the beam scanning. Consequently, even though the received signal for a small swing angle is received properly in-between transmissions, the received signal for a large swing angle such as 15° will be received with a longer delay time, and may be received in conflict with transmission. Furthermore the orbital altitude of a satellite varies due to the relation of the orbital shape to the oblateness of the Earth. These issues can be resolved by adopting a variable pulse repetition frequency (VPRF) [2],[3],[4]. In this paper, several VPRF operations are proposed for the GPM.

2 VPRF for beam swings

In this section, a systematic algorithm of variable PRF is presented for spaceborne weather radars involving cross-track beams scans. To this end, the upper and lower limits of a pulse repetition interval T_{int} for proper receiving should be calculated for the configuration of Fig. 2, in which the minimum and maximum ranges for an arbitrary swing angle θ ($0 \leq \theta \leq \theta_{\mathsf{max}}$) are defined via the delay times t'_1 and t'_2 :

$$t'_2 = 2[\frac{(h(\varphi) + h_{\mathsf{at}} + h_{\mathsf{fl}})(1 + \Delta\theta \cdot \tan|\theta|)}{\cos\theta} + h_{\mathsf{g}}]c^{-1} \quad (1)$$

$$t'_1 = 2[\frac{(h(\varphi) - h_{\mathsf{ob}} - h_{\mathsf{fl}})(1 - \Delta\theta \cdot \tan|\theta|)}{\cos\theta}]c^{-1}. \quad (2)$$

In Eqs. 1 and 2, $h(\varphi)$ denotes the altitude from the geoid as a function of φ, and $\Delta\theta$ represents a beam pointing error of about 0.3°. The other parameters are to be referred in Table 1. The following equation is found to be satisfied to grab the receiving signal between the (n-1)-th and n-th transmissions:

$$(n-1)T_{\mathsf{int}} < t_1 < t_2 < nT_{\mathsf{int}} \quad (3)$$

in which

$$t_1 = t'_1 - 2h_{\mathsf{ex}}c^{-1} - t_{\mathsf{sw}} - \tau_{\mathsf{p}} \quad (4)$$

$$t_2 = t'_2 + 2h_{\mathsf{ex}}c^{-1} + t_{\mathsf{sw}} \quad (5)$$

in which h_{ex} is an extra margin of range, and t_{sw} denotes a dead time during which the RF system switches from transmission to receiving, and vice versa. The pulse duration is represented by τ_{p}. Using these relations, the upper and lower limits of T_{int} can be calculated as shown in Fig. 3 for a fixed orbital angle φ = 80° as a function of the swing angle θ. Figure 4 (a) is a schematic of Fig. 3, in which radar beams are transmitted in the angles θ_{i} (i = 2, 3, 4) discretely. $T_{\mathsf{i\,max}}$ and $T_{\mathsf{i\,min}}$ are the upper and lower limits of T_{int} for a θ_{i}. Then the region of T_{int} common to the adjacent swing angles of θ_{i} and $\theta_{\mathsf{i+1}}$ can be defined by the lines of $T_{\mathsf{i\,i+1\,max}}$ and $T_{\mathsf{i\,i+1\,min}}$ in hatched regions in the figure. The pulse repetition interval $T_{23} \in [T_{\mathsf{23\,min}}, T_{\mathsf{23\,max}}]$ can therefore be applied to both the beam angles of θ_2 and θ_3, and $T_{34} \in [T_{\mathsf{34\,min}}, T_{\mathsf{34\,max}}]$ can be applied to θ_3 and θ_4. On the other hand, there is no common T_{int} existing across over θ_2 and θ_4, indicated by no overlap between the two hatched regions. This problem can be solved by applying a pulse pattern schematically shown in Fig. 4 (b), in which a catching integer $n = 3$ and a sampling number of 8 per a swing angle of θ_{i} ($i = 1, 2, 3, 4$) are assumed for illustration. In the figure, the second half of samplings at θ_2, marked by 1 to 4, and the first half for θ_3, marked by 5 to 8, are operated with the interval of T_{23}, while the second

[1] Corresponding author address: Satoru Kobayashi, Communications Research Lab., Japan; E-mail: satoru@crl.go.jp

half for θ_3, marked by 9 to 12, are operated with T_{34}. It is noted that the transmitted pulses marked by 7 and 8 are received across the transient of T_{23} and T_{34}, however both T_{23} and T_{34} satisfy the relation of $T_{3\,\mathsf{min}} \leq T_{34} < T_{23} \leq T_{3\,\mathsf{max}}$, and are found to be received properly in-between transmission pulses for the swing angle θ_3.

3 Application to the GPM

In the GPM, the Ku-band channel of the dual frequency radar has a swath of 250 km, corresponding to 49 angle bins for a footprint of 5 km diameter along with the maximum swing angle of 17°, while the Ka-band channel has a swath of 100 km, corresponding to 24 angle bins for the same footprint size along with the maximum swing angle of 8.5°.

For this dual frequency operation, pulse patterns are designed to be categorized to three classes in Table 2, all the operations of which have been calculated for the same parameters as in Fig. 3 with a clock frequency of 6 kHz. The first class (1) involves fixed PRF operation. The other two classes are classified to VPRF operations, but should be distinguished in aspect that whether transmission of one of the Ku- and Ka-band channels interferes to receiving of the other channel, or not. The most plausible interference can be considered to occur, when the receiving sidelobe of the Ka-band antenna can not be sufficiently suppressed down at the bi/tri-frequency of the Ku-band. Under this condition, the Ka-band receiving signal will be deteriorated by Ku-band transmission. Inversely if such interference does not exist, the Ku- and Ka-band radars can be transmitted independently with different PRFs to attain the maximum efficient sampling at each channel. This operation will be referred to as the second class (2). On the other hand, in the case that the interference exists, the two radars must be transmitted synchronously to avoid the interference, which will be referred to as the third class (3). In Table 2, the operation denoted by PVPRF is a special case of the class (3), in which the T_{int} is controlled to vary as a function of only the polar orbital angle φ. In other words for a given φ, the values of T_{int} are common for all the swing angles θ.

The operations of the classes (2) and (3) in Table 2 consist of the main and interlace modes. To illustrate these modes, a scanning diagram for the VPRF-A in the class (2) is depicted in Fig. 5. The main mode corresponds to the lanes with the squares marked by 1-49 and 50-98. The interlace mode lanes are in-between the main modes, marked by 38-61 and parts of which are marked by 1-12 and 86-98. The Ku-band channel scans all the points of the main mode from 1 to 49 (or from 50 to 98). On the other hand, the Ka-band channel scans the overlapping points of 13-37 in the main mode lane in synchronization to the Ku-band channel, equivalently with the same VPRF as the Ku-channel. Thereafter the Ka-channel scans the points marked by 38 to 61 in the interlace mode, independently from the Ku-channel that is in the main mode. Eventually both the channels return to scan the points from 62 to 85, again synchronously and so forth. The footprint diagram and the pulse transmission manner of VPRF-B are basically the same as those of Fig. 5, hence the diagram is not illustrated here. For the class (3), the geometrical configuration of the footprint diagram is similar to Fig. 5. However in this class (3), not only the overlapping points of 13-37 but also the points in the interlace mode are scanned by the Ka-band channel synchronously to the Ku-band channel that is in the main mode.

In Table 2, the gains to the fixed PRF (Fix) are tabulated for the VPRF operations. As long as the interference of the Ku-channel to the Ka-channel is ignorable, the operations in the class (2) are advantageous to increase gains by about 2 dB in comparison with the class (1). In case that the interference of both the channels is substantial, an operation in the class (3) should be adopted in stead. As a consequence, adoption of the VPRF is advantageous to increase sampling numbers, enhancing an effective signal-to-noise ratio such as defined in [5] by 1 to 2 dB. If further increase in sensitivity is desired, the frequency agility can be introduced to combine easily to the VPRF [2],[3].

Power consumption is also a key issue to adopt the VPRF that consumes more power at the cost of increasing sampling numbers. Based on a recent evaluation at the CRL, the parameters relating to the VPRF, i.e. pulse repetition frequency, pulse duration and frequency agility, affect only a small portion of the total power, which is mainly consumed by solid state power amplifiers (SSPA). As an example, for the fixed PRF (1) in Table 2 using pulse duration of 1.67 $\mu\,\mathrm{sec}$ with no frequency agility, the SSPAs will consume about 5 Watts, among the total of ≈ 300 Watts in a radar system It means that, even though one of the class (2) is operated with a pulse duration of 3.33 $\mu\,\mathrm{sec}$ and two frequency agility, the total power may increase by at most 30 Watts. Thus on designing the VPRF, we can find some optimally compromised parameters of VPRF for a given power budget.

Acknowledgements

	Fig. 4
switching dead time t_{sw}	15 μsec
observable altitude h_{ob}	20 km
uncertainty in satellite alt. h_{fl}	1 km
extra margin of range h_{ex}	2 km
margin for the Earth oblateness h_{at}	1 km
beam-pointing error $\Delta\theta$	0.3°

Table 1. Operational parameters adopted for Fig. 4.

The authors wish to thank our colleagues, Hiroshi Hanado and Nobuhiro Takahashi for their advices of technical and scientific aspects on the GPM project.

4 References

[1] S. Kobayashi and T. Iguchi, "Variable pulse repetition frequency for the Global Precipitation Measurement Project (GPM)", *IEEE Trans. Geosci. and Remote Sensing*, in press, 2003.

[2] E. Im, S. L. Durden, C. Wu, T.R. Livermore, " The 94-GHz Cloud Profiling Radar for the CloudSat Mission," *2001 IEEE Aereospace Conference*, Big Sky, Montana, pp. 1803-1809, 2001.

[3] J. Awaka, T. Kozu and K. Okamoto, " A feasibility study of rainfall radar for the Tropical Rainfall Measuring Mission, Part 2, Determination of basic system parameters," *Journal of the Communication Research Laboratory*, vol. 35, pp. 111-133, July, 1988.

[4] T. Ihara and K. Nakamura, " A feasibility study of rainfall radar for the Tropical Rainfall Measuring Mission, Part 4, A discussion of pulse compression and adaptive scanning," *Journal of the Communication Research Laboratory*, vol. 35, pp. 149-161, July, 1988.

[5] F.W. Ulaby, R.K. Moore and A.K. Fung, Microwave Remote Sensing, Norwood, MA: Artech House, Inc., ch. 7, pp. 492-495, 1982.

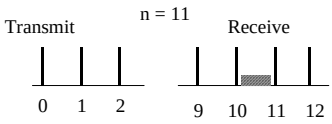

Fig. 1. A schematic of pulse transmission and receiving in a typical space mission. A pulse transmitted on time 0 is received between the 10th and 11th transmission pulses, which defines a catching integer n = 11.

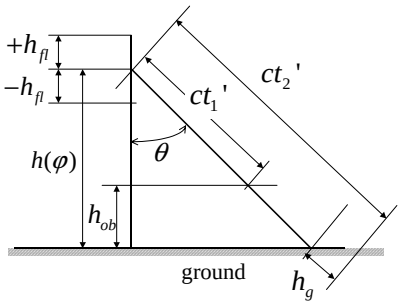

Fig. 2. A geometrical configuration to design the VPRF involving cross-track beam scanning. In this operation, the maximum (ct_2') and minimum ranges (ct_1') are given for an arbitrary swing angle θ.

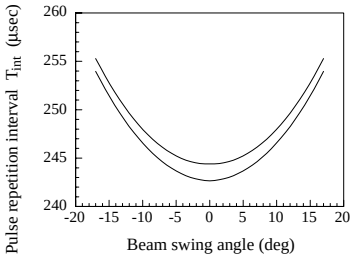

Fig. 3. The upper and lower limits of the pulse repetition interval T_{int} as a function of swing angle θ at the orbital polar angle $\varphi = 80°$. The catching integer $n = 11$ and the parameters in Table 1 are used.

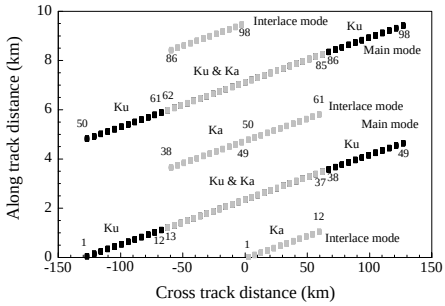

Fig. 5. A footprint diagram for the VPRF-A operation in Table 2. The Ku-band channel scans the entire main mode (1-49 and 50-98) with the sampling number $N_{\mathsf{smp}} = 48$. The Ka-band channel scans the overlapping regions in the main modes (13-37 and 62-85) with $N_{\mathsf{smp}} = 48$ and the interlace mode (38-61) with $N_{\mathsf{smp}} = 52$. In the overlapping regions, both the channels scan synchronously.

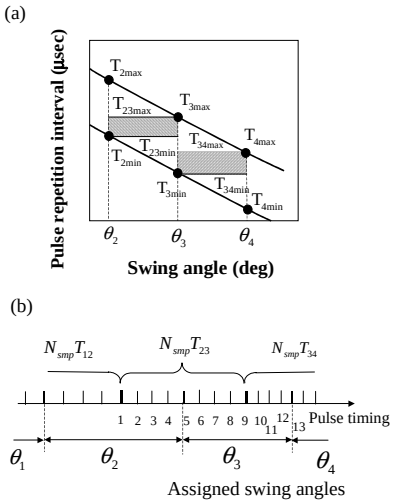

Fig. 4.(a) A schematic of Fig. 3. The common T_{int} for swing angles θ_2 and θ_3 and that of θ_3 and θ_4 are indicated by hatched regions. (b) A pulse pattern for proper receiving across over θ_2, θ_3 and θ_4. The sampling number of 8 and the catching integer $n = 3$ are assumed for illustration.

(1) Fixed PRF

	h_{ob} (km)	N_{smp}	PRF (kHz)	Gain (dB)
(i) Fix	20	20 (n=5)	1.7	x

(2) VPRF with independent transmission of Ku- and Ka-band channels

(i) VPRF-A				
main mode	20	48 (n=11)	4	1.9
interlace mode	19	52 (n=12)	4.5	2.1
(ii) VPRF-B				
main mode	20	48 (n=11)	4	1.9
interlace mode	15	56 (n=13)	5	2.2

(3) VPRF with synchronized transmission of Ku- and Ka- band channels

(i) VPRF-C				
main mode	20	36 (n=8)	2.7	1.3
interlace mode	17	36 (n=8)	2.6	1.3
(ii) PVPRF				
main mode	20	30 (n=7)	2.3	0.9
interlace mode	20	30 (n=7)	2.3	0.9

Table 2. Designs of pulse patterns calculated for the parameters of Fig. 3 without frequency agility. The patterns are categorized to three classes from (1) to (3). h_{ob}: observable altitude. N_{smp}: sampling number per an angle bin. n : catching integer.